



HAL
open science

Aqueous alteration and bioalteration of a synthetic enstatite chondrite

Caroline Avril, Valérie Malavergne, Eric D. van Hullebusch, Fabrice Brunet, Stephan Borensztajn, Jérôme Labanowski, Louis Hennet, François Guyot

► **To cite this version:**

Caroline Avril, Valérie Malavergne, Eric D. van Hullebusch, Fabrice Brunet, Stephan Borensztajn, et al.. Aqueous alteration and bioalteration of a synthetic enstatite chondrite. *Meteoritics and Planetary Science*, 2021, 56 (3), pp.601-618. 10.1111/maps.13641 . hal-03226583

HAL Id: hal-03226583

<https://hal.science/hal-03226583>

Submitted on 28 Oct 2021

HAL is a multi-disciplinary open access archive for the deposit and dissemination of scientific research documents, whether they are published or not. The documents may come from teaching and research institutions in France or abroad, or from public or private research centers.

L'archive ouverte pluridisciplinaire **HAL**, est destinée au dépôt et à la diffusion de documents scientifiques de niveau recherche, publiés ou non, émanant des établissements d'enseignement et de recherche français ou étrangers, des laboratoires publics ou privés.

Aqueous alteration and bioalteration of 1 a synthetic enstatite chondrite

Running title: Alteration and bioalteration of a synthetic enstatite chondrite

Caroline AVRIL¹, Valérie MALAVERGNE^{1*}, Eric D. VAN HULLEBUSCH², Fabrice BRUNET³, Stephan BORENSZTAJN², Jérôme LABANOWSKI⁴, Louis HENNET⁵ and François GUYOT^{6,7}

¹ Université Gustave Eiffel, Laboratoire Géomatériaux et Environnement, EA 4508, UPEM, 5 boulevard Descartes, 77454 Marne-la-Vallée, Cedex 2, France.

² Université de Paris, Institut de physique du globe de Paris, CNRS, F-75005 Paris, France

³ ISTERre, CNRS – Univ. Grenoble Alpes, Maison des Géosciences, BP 53, 38041 Grenoble Cedex 9, France.

⁴ Université de Poitiers, Laboratoire de Chimie et Microbiologie de l'Eau, UMR CNRS 6008, 40 avenue du recteur Pineau, 86022 Poitiers, France.

⁵ Conditions Extrêmes et Matériaux : Haute Température et Irradiation, UPR 3079 CNRS 14 université d'Orléans, 1d avenue de la recherche scientifique, 45071 Orléans Cedex 2, France.

⁶ Muséum National d'Histoire Naturelle, Sorbonne Universités, IMPMC UMR 7590 CNRS, 61 rue Buffon, 75005 Paris, France.

⁷ Institut Universitaire de France

*Corresponding author: Valerie.Malavergne@u-pem.fr

Tel : +33 1 49 32 90 36 ; Fax +33 1 49 32 91 37

Abstract. Understanding the transformations of highly reduced 21 Enstatite Chondrites (EC) in terrestrial environments, even on very short timescales, is important to make the best use of the cosmochemical and mineralogical information carried by these extraterrestrial rocks. Analogues of EC meteorites were synthesized at high-pressure and high-temperature. Then, their aqueous alterations, either abiotic or in presence of the bacteria *Acidithiobacillus ferrooxydans* or *Acidithiobacillus thiooxydans*, were studied under air, at pH~ 2, 20°C and atmospheric pressure. They stayed in batch shaken reactors during 15 days. Reference experiments were carried out separately by altering only one mineral phase among those composing the synthetic EC (i.e., sulfides: troilite or Mg-Ca-rich sulfides, enstatite and Fe₇₀Si₃₀). Composition of the alteration aqueous media and microstructures of the weathered solids were monitored by inductively coupled plasma atomic emission spectroscopy and by scanning electron microscopy, respectively. Alteration sequence of the different mineral components of the synthetic EC was found to occur in the following order: magnesium-calcium sulfides > troilite > iron-silicon metallic phase > enstatite regardless of the presence or absence of the microorganisms. Such small biological effects might be due to the fact that the alteration conditions are far from biologically optimal which is likely the case in most natural environments. The exposed surfaces of an EC meteorite falling on Earth in a wet and acidic environment could lose within few hours their Ca and Mg-rich sulphides (oldhamite and 39 niningerite). Then, in less than one week, troilite and kamacite could be altered. In a wet and acidic environment, only the enstatite would remain intact and would weather on a much slower geological time scale.

43 **Key words:** enstatite chondrite, **aqueous** alteration, bio-weathering, iron oxidizing bacteria, 44 sulfur oxidizing bacteria

1. Introduction

Enstatite chondrites (EC) are among the most reduced materials found in the solar system. They could have played a key role as primitive materials to form the Earth and Mercury (Wänke et al., 1984; Javoy, 1995; Javoy et al., 2010; Malavergne et al., 2010; Zolotov, 2011, 2013; Malavergne et al., 2014). For this purpose, their aqueous alteration on the Earth's surface has been investigated in the present paper either in abiotic oxic conditions or in the presence of aerobic lithoautotrophic bacteria. This study aims to give indications on the fate of these rare materials on the Earth's surface. It also provides original data about oxidative alteration of complex highly reduced materials containing metal phases which is of interest in corrosion studies (Le Forestier and Libourel, 2008; Saheb et al., 2010; Monnier et al., 2010). Moreover, the search for specific signatures of their bio-alteration at the surface of other planetary bodies could be helpful for astrobiological studies. Although there is no published study on the bioweathering of EC, it has been shown previously that alteration of metallic iron from both iron meteorites and carbonaceous chondrites could provide chemical source of energy for microorganisms in aerobic and anaerobic conditions (González-Toril et al., 2005; Gronstal et al., 2009). It is also expected that microorganisms are involved in natural alteration processes of meteorites (e.g. Velbel et al., 1991; Ash and Pillinger, 1995; Barrat et al., 1999; Benzerara et al., 2006). The three main EC forming minerals are FeS (troilite), Fe-Si alloy (kamacite) and enstatite. Numerous literature data exist about troilite weathering (e.g. Steger and Desjardins, 1978; Steger, 1982; Orlova et al., 1989; Thomas et al., 2000; Thomas et al., 2003; Chiriță and Descostes, 2006; Chiriță et al., 2008; Giaveno et al., 2011) showing that the surface of FeS undergoes sulfur enrichment as a result of preferential release of iron upon dissolution. This process can be accelerated with a temperature increase and a pH decrease. There is less literature data about the Fe-Si alloy alteration processes. Ban et al. (1979) showed that the oxidative weathering of Fe-Si alloys was slowed down because of the formation of a SiO₂ passivating layer at the alloy surface, this layer being almost absent when the Si content of the alloy decreased to less than 1wt%. Suzuki et al. (2007) characterized the oxidative alteration products obtained on pure iron and Fe-Si alloy. The main difference between these two systems was the formation of α -FeOOH with Fe-Si alloy rather than β -FeOOH with pure iron. The different studies about enstatite weathering (e.g. Hoch et al., 1996; Chen et Brantley, 1998; Pokrovsky and Schott, 2000; Oelkers and Shott, 2001; Ohnishi and Tomeoka, 2007; Velbel and Barker, 2008) showed the importance of the pH on the weathering processes. The dissolution of enstatite is non stoichiometric under acidic conditions (pH = 2) and its dissolution is faster than at higher pH. Few studies were dedicated to enstatite or pyroxenes bioweathering (Berner and Schott, 1982; Herrera et al., 2004; Benzerara et al., 2004 and 2005; Bassez, 2017). In those studies, the main biological effect was to slow down the alteration kinetics presumably by protection mechanisms of the mineral surface.

More than 400 minerals have been identified in meteorites (Rubin and Ma, 2017). All these minerals were formed by a wide variety of mechanisms, including terrestrial alteration. Moreover, the main factors influencing the terrestrial alteration process of a meteorite include the climate of the area where it fell, its mass, its terrestrial age and its initial porosity (Ouknine et al., 2019). The present study does not have the ambition to explain all the possible terrestrial alteration sequences that can occur in enstatite chondrites but more modestly to focus on the alteration of its three major minerals (metallic alloy, sulfides, enstatite) under aqueous acidic conditions. The minerals produced by weathering in enstatite meteorites include (e.g.: Okada et al., 1981; Rubin, 1997; Nakamura-Messenger et al., 2012; Rubin and Ma, 2017): (1) oxides and hydroxides formed directly from metallic alloys by oxidation and water incorporation (e.g. goethite, ferrihydrite, hematite, etc...); (2) Bassanite, vaterite, calcite and portlandite formed by the decomposition of the sulfides rich in Ca and Mg and a few small patches of an unknown S-rich layer phase were also found; (3) sulfates formed from

troilite (honessite, jarosite) and (4) plethora of phyllosilicates, carbonates and sulfates formed by extensive terrestrial alteration from the silicates and other secondary phases. In the present study, a synthetic equilibrated EC analogue with simplified and well-defined composition and mineralogy was used as a starting material of batch alteration experiments under aqueous acidic conditions. Separate phases constituting the EC analogue were also altered in the same conditions for comparison purposes. Pure cultures of iron oxidizing bacteria (*Acidithiobacillus ferrooxidans*) and sulfur oxidizing bacteria (*Acidithiobacillus thiooxidans*) were used. Abiotic controls were also systematically studied.

2. Experimental and analytical procedures

2.1. Experimental techniques.

2.1.1. EC synthesis.

The synthesis of EC was done in two steps. The first one was the elaboration of a simplified CI chondritic glass. This glass was one of the starting products for the high-pressure and high-temperature synthesis allowing us to obtain a synthetic EC. First, we synthesized a simplified CI chondritic glass (24 wt% Si, 1 wt% Al, 113.4 wt% Fe, 22.1 wt% Mg, 2.2 wt% Ca, 45.9 wt% O) (Thibault and Walter, 1995). This glass was prepared from powdered oxides and carbonates. The starting oxides and carbonates (SiO₂, Al₂O₃, Fe₂O₃, MgCO₃, and CaCO₃, all from GoodfellowTM with a purity > 99.99%) were dried overnight, weighted, mixed in an agate mortar and placed in a platinum crucible. The crucible was placed in a high temperature vertical furnace and heated up to 600°C in 2 hours. Temperature was then held at 600°C for 1 hour to initiate decarbonation. The temperature was then increased up to 1650°C and maintained at this temperature for 2 hours in order to obtain a homogeneous liquid. The experiment was then quenched by dipping the crucible bottom into water. The glass was dark grey and contained some SiO₂ and olivine crystals. Then, this simplified CI glass (74 wt.%) was mixed with FeS (21 wt.%) and pure Si (5 wt.%) (both from GoodfellowTM with a purity > 99.99%). This mixture was used as a starting material for the EC-analogue synthesis and carried out at high pressure and high temperatures. These syntheses were performed at 0.8 GPa and 1350°C (160 hours) in a piston-cylinder apparatus. Experimental details are given in Brunet et al. (2003), Avril et al. (2013) and in Malavergne et al. (2014). After reaction at high temperature and high pressure in piston-cylinder, this material was studied by Raman spectroscopy, transmission and scanning electron microscopy (Avril et al., 2013; Malavergne et al., 2014) and shown to contain the main forming minerals of EC (Fig. 1): enstatite, Fe-Si-alloy (containing between 3 and 6 wt% of Si), SiO₂, troilite FeS, and other Ca-Mg-Fe sulfides. After piston-cylinder syntheses, samples were cut into slices of approximate similar sizes, which were used in the alteration experiments. All samples were characterized before weathering. The relative proportion of each phase was determined before alteration for all the EC slices used for alteration experiments. Based on Scanning Electron Microscopy (SEM), it was possible to estimate the relative area occupied by each phase. We found that the silicate phases (enstatite+SiO₂) occupied between 83-95% of the sample surface, the Fe-Si metal between 1 and 5%, troilite between 1 and 6% and the Mg-Ca-Fe-S-rich sulphide between 2 and 6%. In order to better understand the alteration of this complex multiphasic material, batch alteration experiments were also conducted in the same conditions on pure phases representative of the mineral constituents of the EC analogue (called hereafter “*reference experiments*”). Different “*reference experiments*” were thus performed with enstatite, Fe-Si-bearing alloy, troilite, Mg rich and Ca-rich sulfides.

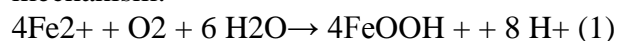
2.1.2. Reference experiments.

We used natural crystals of San Carlos enstatite (MgO = 147.325 wt%, FeO = 7.5 wt%, SiO₂ = 54.4 wt%, Al₂O₃ = 5.6 wt%; corresponding to the ideal formula

Mg_{0.85}Fe_{0.1}Al_{0.05})₁(Si_{0.95}Al_{0.05})O₃), which was prepared as platelets like in EC alteration runs or as powders. Platelets and powder coexisted in the alteration experiments. Specific surfaces were determined by the Brunauer, Emmett and Teller method (BET) with Ar as inert gas. BET method yielded values of 0.55 m²/g for San Carlos enstatite. The choice of using San Carlos enstatite was dictated by the quality and quantity of the starting material available for this study. Moreover, using this enstatite offered the possibility to better understand the alteration of pyroxene containing Fe²⁺ by two lithotrophic bacterial strains and to understand differences in dissolution rates between these experiments and abiotic controls. Moreover, several studies have shown that the difference in dissolution rate between pure ferrous and magnesian poles in silicate phases remains small (e.g. Casey and Westrich, 1992;). At most, this speed could be a little faster if the enstatite contains more iron than magnesium (e.g. Schott and Berner, 1983). The San Carlos enstatites used in this study have a molar Fe/(Fe+Mg) ratio of about 10%, which confirmed that the presence of iron did not radically change the dissolution rates with respect to the pure magnesium pole. In any case, the use of San Carlos enstatite instead of iron-free enstatite did not change our alteration results, as we will see later. Indeed, the enstatite remained the only phase not significantly altered compared to the other phases (metal and sulfides). For FeS and CaS, commercial synthetic powders (Sigma-Aldrich, 99.9 % purity) were used. Specific surface areas of the FeS powders measured by BET yielded values of 0.43 m²/g. Some of the FeS powder was sintered at 0.8 GPa and 1200°C (60 hours, piston cylinder experiments) in order to obtain platelets which were used together with unconsolidated powder in the alteration experiments. CaS powder was sintered at 0.8 GPa and 1200°C (60 hours, piston cylinder experiments) and used in alteration experiment. As pure MgS was not commercially available, we synthesized it at 0.8 GPa and 1200°C (96 hours, piston cylinder experiments) from a mixture of Mg and FeS, through the reaction: Mg + FeS → MgS + Fe, which was characterized by scanning electron microscopy. An Fe₇₀Si₃₀ alloy was synthesized using a levitation apparatus associated with CO₂ laser heating. The first step of this synthesis consisted in the elaboration of pellets from an assemblage of Fe and Si powders. Parts of these pellets were partially melted in a large copper nozzle to obtain roughly spherical shapes. During the second step, these spheres were placed in an aluminium nozzle in order to obtain a stable levitation. The last step was the melting of these levitated spheres during few minutes at 1800°C. In all steps, the levitation 181 chamber was first evacuated and further filled with pure Ar (with less than 0.05 ppm of oxygen) in order to prevent oxidation of Fe or Si. The laser heating levitation procedure is described in Hennet et al. (2006). After the levitation synthesis procedure, the metallic spheres were cut into two halves of similar size. A single half sphere was used in each alteration experiment after a characterisation by scanning electron microscopy.

2.1.3. Bacterial cultures.

Chemolithoautotrophic iron- or sulfur- oxidizing bacteria, *Acidithiobacillus ferrooxidans* (*A. ferrooxidans*, *AF*) and *Acidithiobacillus thiooxidans* (*A. thiooxidans*, *AT*) were used in the biotic experiments. These bacteria were purchased from the Leibniz Institute German Collection of Microorganisms and Cell Culture (DSMZ). These bacteria are considered to be analogs of lithoautotrophic microorganisms contemporary of the first oxygenic phototrophic organisms (Cairns-Smith et al., 1992; Guiliani et al., 1997). They are known to play a role in the formation of acid mine drainage from sulfidic mine wastes (e.g. Nordstrom and Southam, 1997). The chemical reactions describing bacterial oxidation of soluble Fe²⁺ and/or of a sulfide AS (A= Ca²⁺, Mg²⁺ or Fe²⁺) are schematically without prejudging the actual mechanism:



Altogether these reactions yield highly acidic conditions which prevail for example in acid mine drainages. Locally, when such reactions occur in poorly buffered media with low fluid circulation, pH might become quite low and thus strongly enhance mineral dissolutions. This explains the colonization of such environments by acidophilic micro-organisms such as *A. ferrooxidans* and *A. thiooxidans* and provides a justification for performing tests of this study at pH of ≈ 2 . The mechanisms are far more complex than overall balances (1) and (2). Briefly, under acidic conditions, Fe(III) interacts abiotically with sulfides and other species of sulfur (sulfide, elemental sulfur, polysulfide, thiosulfates) in order to oxidize them in sulfate. *A. ferrooxidans* (DSM 14882) was cultivated at 20°C and pH \sim 2 and shaken at 100 rotation per minute. *A. ferrooxidans* growth media consist of: 0.2 g/L K₂HPO₄, 0.4 g/L (NH₄)₂SO₄, 0.4 g/L MgSO₄·7 H₂O, 8 g/L FeSO₄·7H₂O, 1 mL/L solution of trace elements (from Stergar and Zagorc Koncan, 2002) (Table 1) and distilled water. *A. thiooxidans* (DSM 14887) was cultivated at 20°C and pH \sim 4.5 and shaken at 100 rpm. *A. thiooxidans* growth medium consisted of 0.3 g/L (NH₄)₂SO₄, 0.5 g/L MgSO₄·7H₂O, 0.018 g/L FeSO₄·7H₂O, 0.25g/L CaCl₂·7H₂O, 10 g/L Na₂S₂O₃ sodium thiosulfate, 1 mL/L solution of trace elements (from Stergar and Zagorc Koncan, 2002) and distilled water. The bacteria were separated from their culture media by successive 215 filtrations. The culture media with bacteria were initially filtered using 10 μ m pore size paper filter to separate out the iron oxy-hydroxide precipitates from the media and bacteria. The filtrate was collected and then, filtered again using an autoclaved 0.22 μ m polycarbonate filter to collect the bacterial cells. This filter was flushed with several mL of distilled water to remove residual dissolved Fe from the bacterial cells. The polypropylene tube containing the filter with bacterial cells was placed in an ultra sound water bath (Santelli et al., 2001). The tube solution was then examined by the Gram staining method for bacterial cells and for presence of iron precipitates.

2.1.4. Alteration experiments.

Experiments were carried out in batch reactors shaken at 100 rotation per minute for 10-15 days at 20°C. The reactors were exposed to air during the experiment. Samples were placed in perforated polypropylene tubes, which were added to 75 mL of solution in acid-washed and sterilised polycarbonate flasks (Fig. 2). The Growth Medium (GM) solutions used in all biotic and abiotic experiments consisted of 84 mg/L NaHCO₃, 132 mg/L (NH₄)₂SO₄, 17.4 mg/L K₂HPO₄ and filtered ultrapure water. This medium composition was chosen to provide traces of inorganic nutrients required by the lithoautotrophic microorganisms without severely complicating the solution chemistry in the dissolution experiments, i.e. to avoid most sulfate and phosphate precipitation. As with the bacterial strain culture medium, the culture medium for the experiment is enriched to 1 mL.L⁻¹ with a dilute solution of trace elements (Table 1) and then adjusted close to 2 units with dilute H₂SO₄ (Santelli et al., 2001). The sources of iron and reduced sulfur necessary for *A. ferrooxidans* and *A. thiooxidans* were not included in the composition of this culture medium. The purposes were indeed: (i) to deprive the bacteria of elements essential to their metabolism so that they could obtain them from our samples, (ii) to be in conditions simulating a terrestrial alteration in acidic condition. The bacteria in our study were thus under stress and not in optimal conditions for their growth. Duplicates experiments were performed for each system (i.e. “reference experiments” and EC analogue), except for the alteration of synthetic EC by *A. thiooxidans*.

2.2. Characterization and analytical procedures

The pH measurement was taken every day. In each experiment, 5 mL of aqueous samples were collected each day over 15 days using micropipette. Equivalent volume of fresh medium was added after sampling to maintain constant solid/liquid ratio. Aqueous samples were filtered through a PTFE filter with a pore size of 0.22 μ m and then analyzed by inductively

coupled plasma atomic emission spectrometry (ICP-AES, Perkin-Elmer Optima 6300) for Mg, Fe and Si. The analytical uncertainties in the measurements were below 27% based on repeated analyses of standard solutions.

Recovered weathered samples were stored at 30°C during 24-48 hours. Then, they were fixed on an adhesive carbon support, carbon-coated, and studied with a Scanning Electron Microscope (SEM, ultra55, Zeiss, operating at 15 kV). Controls before alteration were observed as well. Qualitative chemical analyses were acquired by EDX (energy dispersive X-ray analysis, Silicon Drift Detector, Bruker). Initial dissolution rates of each mineral (Table 2) were calculated from the ICP-AES measured concentrations obtained during the first hours, for which linear trends were observed.

3. Results

The results for all the systems studied in this study are given in Figs. 3 - 10. The Fe, Mg and Si concentrations in synthetic EC alteration solutions are given in Fig. 3 a-c. These concentrations increased during the first 167 hours; then this increase slowed down but lasted until the end of the experiment. The measured rates were affected by a dilution effect (as will be discussed in more detail for the "reference experiments" later in this section). This dilution effect did not change the ratios between elements. In all experiments, pH was stable between 2.2 and 2.3. The initial release rates of Mg, Fe and Si in the solutions were similar in biotic and abiotic experiments but some differences were observed in the end values. The evolution of [Mg]/[Si] and [Fe]/[Si] molar ratios in the solution is shown in Fig. 3. Compared to the initial EC composition ([Mg]/[Si]_{initial EC} = 0.84), Mg was released preferentially compared to Si (see Fig. 3d). Fe was more released in the solution than Si. [Fe]/[Si] molar ratios were between $\cdot 6$ and $\cdot 8$ in alteration experiments (Fig. 3e) whereas [Fe]/[Si]_{initial EC} in the EC starting sample was of 0.74. SEM images of the synthetic EC recovered after 14 days from the different experiments are shown in Fig. 4. Few tiny sulfates and phosphate mineral precipitates were observed on the surfaces of each phase (silicates, metal and sulfides). Bacterial activity (i.e. turbidity in the medium, biofilm and cells observed on the mineral surfaces, Fig. 4j-k, Fig. 6c, Fig. 8c and Fig. 10c) was observed in the EC experiments and in most "reference experiments" inoculated with *A. ferrooxidans* and *A. thiooxidans* showing that some Fe²⁺ and S²⁻ coming from the EC analogue or from single phases could be used for bacterial respiration. In those experiments, the presence of biofilms was confirmed by high C content phases at the surface of minerals detected by EDXS analyses (Fig. 4j and Fig. 8c). No bacterial activity was observed in the "*A. thiooxidans* enstatite *reference experiments*". *A. thiooxidans* was therefore considered 281 at best as dormant or at worst as dead in these experiments.

a) (Mg,Ca,Fe)S sulfides.

In EC analogue, all these phases were completely replaced by dissolution holes containing sulfates (Fig. 4a, 4b, 4c, 4g, 4h), tiny globules of iron oxides or hydroxides and sometimes needles of iron-magnesium sulfates (Fig 4b, 4f). These sulfate needles were less dense in biotic conditions as shown in Fig. 4b and Fig 4c. These observations were in agreement with those performed with CaS and MgS dissolution experiments ("*CaS-MgS-reference experiments*") which were the most rapidly altered of all the runs conducted in this study.

b) FeS-Troilite.

In EC analogue, most of these FeS sulfide grains were dissolved and replaced by dissolution holes containing mainly sulfates and iron oxides/hydroxides (Fig. 4a, 4b, 4c, 4g-i). In the case of alteration by *A. thiooxidans*, alteration patches containing iron oxides/hydroxides and

elemental S (Figure 4e) were observed. These observations are in agreement with the results obtained in the “FeS reference experiments” (Fig. 5 and 6). The iron concentrations of the solution present in the “FeS reference experiments” are given in Fig. 5 and the typical microstructures shown in Fig. 6. The surfaces of abiotically altered troilite were covered with a layer of secondary phases, mostly iron oxides and/or hydroxides and iron phosphates (Fig. 6a). This layer was not recovered after bioweathering with *A. ferrooxidans*. After bioweathering with *A. thiooxidans*, patches of iron sulfates remained strongly adhesive to the samples (Fig. 6b). In the troilite reference experiments Fe-rich-sulfates were observed only with *A. thiooxidans* (Fig. 6b) while they were characterized in the synthetic EC system in both biotic and even in abiotic samples (Fig. 4b-c-f). This difference was likely due to the presence of Mg-Ca-rich sulfides in synthetic EC as FeS and Mg-Ca-rich sulfides were most often in direct contact (Fig 3 a-d). The filamentous texture observed in EC analogue differed also from the patch textures in “FeS reference experiments” with *A. thiooxidans* (Fig. 4b-c and Fig. 6b). Then, the textures that formed during alteration of FeS depend on the multiphase of the material.

c) Fe-Si alloy.

In EC analogue experiments, the surface of Fe-Si alloy was covered with silica (Fig. 4a, 4g-i), whereas in biotic experiments, the metal was also covered with iron oxides and/or hydroxides in the form of tiny globules (Fig. 4d, 4g-i). Biofilms were also observed (Fig. 4j). These observations were very similar to those obtained with the “Fe-Si alloys reference experiments” (Fig. 8).

After 14 days in abiotic conditions in the “*Fe-Si alloys reference experiments*”, the surface was completely covered with a SiO₂ layer along with underlying iron-silicon alloy (Fig. 8a). After bioweathering with *A. ferrooxidans* and with *A. thiooxidans*, the sample surfaces of these “*Fe-Si alloys reference experiments*” were only partially covered by a SiO₂ layer (Fig. 8b). SiO₂ precipitation during Fe-Si alloy dissolution was already described in Ban et al. (1979). Tiny iron phosphates were also observed at the surface of this layer, which were not stable under the electron beam. Under the SiO₂ layer, iron oxides and/or hydroxides formed (Fig. 8b) with *A. ferrooxidans* and *A. thiooxidans*. Such oxidation of metallic iron by *A. ferrooxidans* was already reported in the literature (e.g. Magnin et al., 1994).

d) Enstatite.

Except for small deposits of tiny phosphates and sulfates, enstatite surfaces were relatively unmodified after alteration in EC analogue experiments. Also, their compositions were similar before and after alteration in all experiments. The surface microstructures and elemental compositions were consistent with a moderate alteration of enstatite. The surfaces of enstatite in EC analogue display the presence of small deposits of tiny phosphates and sulfates that were very similar to those observed in the “*enstatite reference experiments*”. Fe, Mg and Si concentrations in the aqueous solutions of the enstatite alteration experiments (*reference experiments*) are given in Fig. 9. The surface of enstatite millimeter-sized crystals recovered after 15 days from the different experiments did not show specific features except for some corrosion pits and the presence of some tiny sulfates and phosphates (Fig. 10). The corrosion pits were less numerous and less deep at the end of biotic experiment with *A. ferrooxidans* than at the end of other ones. We remind here that absence of clear signs of bacterial activity was observed for *A. thiooxidans*, which may not totally exclude survival of these bacteria in those conditions.

4. Discussion

a) Dissolution rates in “reference experiments” CaS and MgS dissolution.

A total dissolution of CaS and MgS was observed by optical microscopy in less than 10 hours, depending on the exact thickness of the slice of the sample. These phases have the fastest dissolution among the phases investigated in this study.

FeS dissolution. It also occurred quite fast. However, despite the fact that a plateau has been reached (Fig. 5), a certain amount of FeS persists in the samples (Fig. 6). Thomas et al. (2000) have shown that for similar pH and temperatures, troilite dissolution rates exceeded 10-8 mol/cm²/s, i.e. 100 times faster than in our “*FeS reference experiments*”. This difference could be due to differences in oxygen concentration between this study and that of Thomas et al. (2000) who used deoxygenated solution obtained by purging with Ar. In the present study, some minor oxidation of iron (II) released to solution and subsequent precipitation of iron (III) occurred likely in the initial stages possibly diminishing soluble iron concentrations in comparison with Thomas et al. (2000). This is consistent with the observation of numerous iron oxides/hydroxides and sulfates at the surface of altered FeS in this “*FeS reference experiments*” (Fig. 6) and in EC analogues (Fig. 4a-b-c-d-g). This is also in agreement with previous results from literature (e.g. Bassez, 2017). There is an abundant literature about production of Fe³⁺ upon interaction of sulfides with *A. ferrooxidans* or related strains in the context of acid mine drainages (e.g. Evangelou, and Zhang, 1995; Wang and Zhou, 2012). The slight decrease on the plateau observed in Fig. 5 for the Fe contents in solution after 20 hours of experiment is actually due to a dilution effect. Indeed, we took 5 ml of solution every 24 hours (replaced by 5 ml of "fresh" solution). Thus, after a dilution calculation of the Fe contents in the solution, we believe that that Fe contents would have continued to increase slightly after 20 hours and up to the end of the experiments.

Fe₇₀Si₃₀ alloy dissolution. Dissolution of pure Fe₇₀Si₃₀ alloy (“*Fe-Si alloys reference experiments*”) was not stoichiometric (Fig. 7). [Fe]/[Si] molar ratio was about two times larger than the stoichiometric one ([Fe]/[Si]_{stoichiometric} = 2.3 and [Fe]/[Si]_{measured} = 4.4) (Fig. 7c) indicating preferential Fe release to the solution. The decrease in the Fe and Si contents observed in Fig. 7 after 100 hours of experiment is due to a dilution effect of the medium due to the sampling of 5 ml every 24 hours (replaced by "fresh" solution). Thus, after a dilution calculation of the Fe and Si contents in the solution, it appears that Fe and Si were indeed constant or increased slightly between 100 hours and the end of the experiments. Finally, the fact that the Fe/Si ratio remained globally constant after 100 hours in our experiments indicates that the relative variations of these two elements remained the same until the end of the experiments. A relatively thick layer of silica was observed over almost the entire surface of the abiotic samples, leaving very little alloy still directly observable (Fig. 8a). For biotic samples, this silica layer did not cover the alloy surface as much. On the contrary, part of the alloy was still directly observable, as well as the formation of iron oxides and/or hydroxides (Fig. 8b). Biofilms were also observed (Fig. 8c).

Enstatite dissolution. Dissolution of enstatite seemed to be not stoichiometric in both biotic and abiotic experiments. [Mg]/[Si] and [Fe]/[Si] molar ratios in the solution are about two times larger than the corresponding ratios in the San Carlos enstatite starting material ([Mg]/[Si] = 0.9 and [Fe]/[Si] = 0.1) (Fig. 9e and 9f). Oelkers and Schott 383 (2001) found that the initial dissolution of enstatite was not stoichiometric: Mg dissolved faster than Si at pH=2. After about 50 hours, a steady state was reached and stoichiometric dissolution was observed. Again the Mg, Fe and Si contents slight decrease observed after 175 hours are due to a dilution effect. We obtained the same values as those measured at the end of the

experiment for Mg and Si, i.e. around 2 mg/L for Mg and around 1 mg/L for Si. The ratios ($[Mg]/[Si]$ and $[Fe]/[Si]$) are almost constant after 175 hours, indicating that the relative contents of these 3 elements remained constant. The oxic atmosphere in our enstatite dissolution experiments may help to explain the difference with the data from Oelkers and Schott (2001). These conditions could decrease the dissolution rates of iron-bearing silicates due to the formation of ferric oxides (e.g. Bassez, 2017). Finally, a precipitation of SiO₂ due to the SiO₂-saturated solution results in a high Mg/Si ratio in the aqueous solution. Dissolution of pure enstatite occurred at initial rates similar to those published in the literature and reported in Table 3. Enstatite dissolution was slow and its surface was only slightly affected in the experiments (Fig. 10).

b) Coherence between the results of the reference experiments and the EC analogue.

The order of dissolution observed in the synthetic EC is consistent with those characterized in the *reference experiments* (c.f. Table 2). Indeed, under both biotic and abiotic conditions and among the five separated mineral phases that were investigated here (CaS, MgS, troilite, Fe₇₀Si₃₀ alloy and natural enstatite; Table 2), Mg-Ca-rich sulfides dissolved the fastest, well before FeS, then Fe-Si alloy and finally the enstatite at a much slower rate than the other phases.

Dissolution of *reference* Fe₇₀Si₃₀ alloy was slower than that of pure troilite and Ca-Mg-rich sulfides, in agreement with the order of dissolution rates observed in the textures of altered EC analogue. The dissolution was non stoichiometric and characterized by preferential release of iron. This is consistent with the precipitation of SiO₂ observed on the alloy surfaces both in the EC analogue and in the pure *Fe-Si alloy reference experiments* (Fig. 4 and Fig. 8). The moderate alteration of the enstatites in the EC analogue is consistent with the slow dissolution rate measured in *reference experiments*. The surface microstructures and elemental compositions observed in synthetic EC are consistent with a moderate alteration of the enstatites. The surfaces of enstatite in EC analogue with the presence of small deposits of tiny phosphates and sulfates were very similar to those observed in the *enstatite reference experiments* (Fig. 10). As mentioned above, using an iron-bearing San Carlos enstatite did not change the order of the observed alterations: the enstatite (with or without iron) would always be the last to be altered here. The filamentous texture of the Mg-Fe bearing sulfates associated to cocoon-shaped iron oxides/hydroxides (Fig. 4b, e), resulting from the alteration of sulfides, is interesting for astrobiological issues. These alteration textures could be mistaken with bacterial or fungal remnants. This was particularly spectacular in Fig. 4b, which corresponds to an entirely abiotic experiment. In all cases sulfide oxidation into sulfates in natural settings will locally generate acidic pH's akin to those used in the present study.

c) Inter-relation of phases during the EC alteration.

Although enstatite represents about 85% of the surface exposed to alteration in the EC analogue, the surface dissolution of enstatite considering these rates would contribute to a maximum of 35 μ g/L of Si and 10 μ g/L of Mg, well below the saturation of SiO₂. The surface dissolution of the iron-silicon alloy, which dissolved faster but was in small amounts, would not better explain the reaching of SiO₂ saturation in the EC experiments. It is therefore highly probable that volume dissolution (i.e., formation of deep corrosion pits in the EC analogue platelet samples thus allowing to reach phases within the volume of the sample) of Mg-Fe-Ca sulfide grains explains the magnesium contents in these solutions and that values of dissolved silicon are best explained by a volume dissolution of the Fe-Si alloys.

d) Specific biological effects?

Past studies have indicated the possibility of microstructural and/or chemical specificities in the presence of *A. thiooxidans* and *A. ferrooxidans* with minerals relevant to this study. For example, the formation of iron sulfate patches with *A. thiooxidans* was observed in several experiments (Edwards and Rutenberg, 2001), as well as the oxidation of metallic iron by *ferrooxidans* (e.g. Magnin et al., 1994) or the production of Fe³⁺ upon interaction of sulphides with *A. ferrooxidans* or related strains in the context of acid mine drainages (e.g. Evangelou, and Zhang, 1995; Wang and Zhou, 2012). We therefore wondered whether such chemical and mineralogical changes could have a strong influence on reduced systems such as EC.

First, in the experiments performed in the present study, iron oxides or sulfates occurred sometimes as patches (up to ~80 μ m in diameter) with *A. thiooxidans* in “*FeS reference 446 experiments*” or in “*Fe-Si alloy reference experiments*” and in synthetic altered EC (Fig. 4e and 447 Fig. 6b). These microtextures were possible signatures of this biological activity. These 448 changes in microstructures have no obvious consequences on the bulk chemistry of our systems 4since there is no significant nor strong variation between abiotic and biotic systems (Fig. 3, Fig. 450 5, Fig. 7). It should be noted, however, that even under stress, the bacteria showed signs of life in a more or less direct way with the turbidity in 451 the medium, the formation of biofilms and the observation of bacterial cells (Fig. 4j-k, Fig. 6c, Fig. 8c and Fig. 10c). Second, the only significant chemical variation between the abiotic and biotic systems occurs in the “*Fe-Si alloy reference experiments*” (Fig. 7) with a decrease of the alteration rate of about 20% in the abiotic system. These variations are certainly related to the silica layer that covers almost the entire surface of abiotic samples whereas it covers on average less than half of the surface of biotic samples. In addition, another major difference between our systems with and without bacteria is the formation of iron oxides/hydroxides in the presence of bacteria. These oxides were absent or negligible in the abiotic case. Oxidation of iron from the Fe₇₀Si₃₀ alloy by *A. thiooxidans* was not expected: this bacterial strain might oxidize iron using intermediate reactive species possibly formed in Fenton-like reactions. Third, in the present study, initial dissolution rates of the different minerals are not significantly different between abiotic experiments and those in presence of the two bacterial strains (Table 2 and Table 3). The weakness of this effect may be related to the sub-optimal physiological state of the bacteria present in our experiments. Significant kinetic differences are observed only in the case of the Fe-Si alloy.

Finally, despite the fact that the bacteria present in our study were not in an optimal environment and were in a state of stress, throughout our experiments we observed evidence for their biological activity in most experiments (except for the experiment done with *A. thiooxidans* with enstatite). Even if the bacterial effect on phase dissolution kinetics is weak in the present study, we observed a significant effect on the appearance of certain surfaces (Fig. 4c, 4e or 4i for example). These potential biosignatures at the surface of biologically-altered enstatite chondrites should be investigated further.

e) General comments on the EC alteration processes.

The silicon concentration in the solution of the EC experiment is consistent with the Si saturations (\approx 1 mg/L of Si) also observed in the solutions of the enstatite and Fe₇₀Si₃₀ experiments. However, these values are not all strictly equal (range between 0.5 mg/L and 1.7 mg/L of Si) which suggests that details of the solutions compositions and redox states strongly influence the saturation value of the silica-rich phases present in the different experiments. We observed two textural differences in biotic and abiotic experiments performed with synthetic EC: on sulfide surfaces with *A. thiooxidans* (alteration patches

containing iron oxides/hydroxides and elemental S) and on the metal surfaces (covered with iron oxides and/or hydroxides in the form of tiny globules).

Finally, even if sulphides represent only 8 to 11 vol% of EC, they are 485 the ones that will govern the first step of EC alteration over short periods of time (from a few hours to a few days, Table 2). The second phase of alteration will be controlled by enstatite on a geological time scale. The complex 3D structure of the sulphides in EC might lead to a rapid 3D alteration of these phases even at significant depth below initially exposed surfaces of the meteorite.

f) How do we interpret our results in light of previously published studies on terrestrial meteorite alteration?

By comparing our results with those in the literature (e.g.: Okada et al, 1981; Rubin, 1997; Nakamura-Messenger et al., 2012; Rubin and Ma, 2017), we found that our experiments replicated some of the characteristics already observed with the formation of: (i) iron-rich oxides and hydroxides from the metal alloy and sulfides; (ii) sulphates and elemental S mainly from troilite and other Mg-rich and Ca-rich sulfides. As our experiments were of limited duration (15 days) compared to the alteration time of the natural samples, we did not observe the presence of phyllosilicates associated to the alteration of the enstatites.

However, phyllosilicates have often been characterized in extensively altered meteorites on the Earth's surface (e.g. Rubin and Ma, 2017 and references therein). Thus, in conclusion of this comparison, our experiments were able to reproduce only the major families of minerals resulting from rapid (i.e. less than one month) alteration processes.

4. Conclusions

This study shows that the dissolution kinetics of a synthetic enstatite chondrite (EC) under acidic-oxic conditions is governed first by the rapid dissolution of Mg-Ca-rich sulfides, then of troilite (FeS), then of the Fe-Si metallic phase, while these phases represent between 4 to 17 vol% of the synthetic EC. Dissolution of pyroxenes occurs on slower timescales. This order of dissolution rates is consistent with that derived from data on separate mineral phases constitutive of natural EC. Initial dissolution rates of the separate mineral phases and alteration microstructures were found to be similar between abiotic and biotic systems. Similarly, the different bacterial strains did not reveal any significant differences. These only slight differences might be related to a non-optimal physiological state of the bacteria in these experiments which might be the case in the media of alteration of enstatite chondrites in terrestrial environments. The only clear differences in alteration microstructures between abiotic and biotic cases were evidenced in the case of Fe-Si alloys: the presence of iron oxides together with SiO₂ was observed only in biotic experiments whereas only SiO₂ was found in abiotic conditions. Finally, FeS, Fe-Si alloys and Mg-Ca-rich sulphides present in a natural EC falling on Earth in acidic aqueous environment 519 (pH ~ 2) would be altered quickly: in less than one week, while enstatite would survive very much longer time.

5. Acknowledgments

The authors would like to warmly thank the associate editor and the two reviewers who helped to improve the manuscript and especially the presentation of the results and the quality of the discussion of this study.

References

- Avril C., Malavergne V., Caracas R., Zanda B., Reynard B., Charon E., Bobocioiu E., Brunet F., Borensztajn S., Pont S., Tarrida M., Guyot F. 2013. Raman spectroscopic properties and Raman identification of CaS-MgS-MnS-FeS-Cr₂S₃ sulfides in meteorites and reduced sulfur-rich systems, 48: 1415-1426.
- Ash R. D. and Pillinger C. T. 1995. Carbon, nitrogen and hydrogen in Saharan chondrites: The importance of weathering. 30:85-92.
- Ban, T., Bohnenkam, K., Engell, H.J. 1979. The formation of protective films on iron-silicon alloys. *Corros. Sci.* 19: 283-293.
- Barrat J. A., Gillet P., Lesourd M., Blichert-Toft J., and Poupeau G. R. 1999. The Tatahouine diogenite: Mineralogical and chemical effects of sixty-three years of terrestrial residence. 34:91-97.
- Benzerara, K., Chapon, V., Moreira, D., López-García, P., Guyot, F., Heulin, T., 2006. Microbial diversity on the Tatahouine meteorite. 41:1249-1265.
- Brunet, F., Bagdassarov, N., Miletich, R., 2003. Na₃Al₂(PO₄)₃, a fast sodium conductor at high pressure : in-situ impedance spectroscopy characterisation and phase diagram up to 8 GPa. *Solid State Ionics* 159: 35-47.
- Cairns-Smith, A.G., Hall, A.J., Russel, M.J., 1992. Mineral theories of the origin of life and an iron sulfide example. *Origins life evolution biosphere* 22: 161-180.
- Casey, W. H., Westrich, H. R., 1992. Control of dissolution rates of orthosilicate minerals by divalent metal-oxygen bonds. *Nature* 355: 157-159.
- Evangelou, V. P., Zhang, Y. L. (1995). A review: pyrite oxidation mechanisms and acid minedrainage prevention. *Critical Reviews in Environmental Science and Technology* 25:141-199.
- González-Toril, E., Martínez-Frías, J., Gómez, J.M.G., Rull, F., Amils, R. 2005. Iron meteorites can support the growth of acidophilic chemolithoautotrophic microorganisms. *Astrobiology* 5: 406-414.
- Gronstal, A., Pearson, V., Kappler, A., Dooris, C., Anand, M., Poitrasson, F., Kee, T.P., Cockell C.S., 2009. Laboratory experiments on the weathering of iron meteorites and carbonaceous chondrites by iron-oxidizing bacteria. 44: 2, 233-247.
- Guiliani, N., Bengrine, A., Borne, F., Chippaux, M., Bonnefoy, V., 1997. Alanine-tRNA synthetase gene of the extreme acidophilic chemolithoautotrophic *Thiobacillus ferrooxidans* is highly homologous to *alaS* genes from all living kingdoms but cannot be transcribed from its promoter in *Escherichia coli*. *Microbiology* 143: 2179-2187.
- Hennet, L., Pozdnyakova, I., Bytchkov, A., Cristiglio, V., Palleau, P., Fischer, H.E., Cuello, G.J., Johnson, M., Melin, P., Zanghi, D., Brassamin, S., Brun, J.F., Price, D.L., Saboungi, M.L., 2006. Levitation apparatus for neutron diffraction investigations on high temperature liquids. *Rev. Sci. Instrum.* 77: 053903-053907.
- Javoy, M., 1995. The integral enstatite chondrite model. *Geophys. Res. Lett.* 22 : 2219-2222.
- Javoy, M., Kaminski, E., Guyot, F., Andraut, D., Sanloup, C., Moreira, M., Labrosse, S., Jambon, A., Agrinier, P., Davaille, A., Jaupart, C., 2010. The chemical composition of the Earth: Enstatite chondrite models. *Earth Planet. Sc. Lett.* 293: 259-268.
- Le Forestier L., Libourel G., 2008. High temperature behavior of electrostatic precipitator ash from municipal solid waste combustors, *J. Hazard. Mater.* 154: 373-380.
- Magnin, J.P., Garden, J., Ozil, P., Pathe, C., Picq, G., Poignet, J.C., Schoeffert, S., Vennereau, P., Vincent, D. 1994. Preparation of porous materials by bacterially enhanced corrosion of Fe in iron-titanium hot-pressed plates *Materials Science and Engineering A*. 189: 165-172.
- Malavergne V, Cordier P., Righter K., Brunet F., Zanda B, Addad A., Smith T., Bureau H., Surblé S., Raepsaet C., Charon E. 2014. How Mercury can be the most reduced terrestrial planet and still store iron in its mantle, *Earth Planet. Sci. Lett.* 394: 186-197.

- Malavergne, V., Toplis, M.J., Berthet, S., Jones, J. 2010. Highly reducing conditions during core formation on Mercury: Implications for internal structure and the origin of a magnetic field. *Icarus* 206: 199-209.
- Monnier J., Neff D., Réguer S., Dillmann P., Bellot-Gurlet L., Leroy E., Foy E., Legrand L., Guillot I., 2010. A corrosion study of the ferrous medieval reinforcement of the Amiens cathedral. Phase characterisation and localisation by various microprobes techniques. *Corrosion Science* 52: 695-710.
- Nakamura-Messenger, K., Clemett, S.J., Rubin, A.E., Choi, B.-G., Zhang, S., Rahman, Z., Oikawa, K., Keller, L.P., 2012. Wassonite: a new titanium monosulfide mineral in the Yamato 691 enstatite chondrite. *Am. Miner.* 97, 807–815.
- Nordstrom, D.K., Southam, G., 1997. Geomicrobiology of sulfide mineral oxidation, *Geomicrobiology: Interactions Between Microbes and Minerals, Reviews in Mineralogy*. 35, Mineralogical Society of America, Washington D.C, J.F. Banfield, K.H. Nealson (Eds.) 361–390.
- Oelkers, E.H., Schott, J., 2001. An experimental study of enstatite dissolution rates as a function of pH, temperature and aqueous Mg and Si concentration, and the mechanism of pyroxene/pyroxenoid dissolution. *Geochim. Cosmochim. Acta* 65: 1219-1231.
- Okada, A., Keil, K., Taylor, G.J., 1981. Unusual weathering products of oldhamite parentage in the Norton County enstatite achondrite. *Meteoritics* 16, 141–152.
- Ouknine, L., Khiri, F., Ibhi, A., Heikal, M., Th S., Saint-Gerant, T., Medjkane M., 2019. Insight into African meteorite finds: Typology, mass distribution and weathering process. *J. African Earth Sciences* 158, 103551.
- Rubin, A.E. and Ma, C., 2017. Meteoritic minerals and their origins, *Chemie der Erde* 77:325-385.
- Rubin, A.E., 1997. Mineralogy of meteorite groups. *Meteorit. Planet. Sci.* 32, 231–247.
- Saheb M., Descostes M., Neff D., Matthiesen H., Michelin A., Dillmann P., 2010. Iron corrosion in an anoxic soil: comparison between thermodynamic modelling and ferrous archeological artefacts characterised along with the local in situ geochemical conditions, *Applied Geochemistry* 25: 1937-1948.
- Santelli, C.M., Welch, S.A, Westrich, H.R., Banfield, J.F., 2001. The effect of Fe-oxidizing bacteria on Fe-silicate mineral dissolution. *Chem. Geol.*180: 99-115.
- Schott, J., Berner, R. A., 1983. X-ray photoelectron studies of the mechanism of iron silicate dissolution during weathering, *Geochim. Cosmochim. Acta* 47: 2233-2240.
- Stergar, V., Zagorc Koncan, J., 2002. The determination of anaerobic biodegradability of pharmaceutical waste using advanced bioassay technique. *Chemical and Biochemical Engineering* 16: 17-24.
- Thibault, Y., Walter, M., 1995. The influence of pressure and temperature on 616 the metal-silicate partition coefficients of nickel and cobalt in a model C1 chondrite and implications for metal segregation in a deep magma ocean. *Geochim. Cosmochim. Acta* 67: 991-1002.
- Thomas, J.E., Smart, R.St.C., Skinner, W.M., 2000. Kinetic factors for oxidative and non oxidative dissolution of iron sulphides. *Mineral. Eng.* 13: 10-11, 1149-1159.
- Velbel M. A., Long D. T., and Gooding J. L. 1991. Terrestrial weathering of Antarctic stone meteorites: Formation of Mg carbonates on ordinary chondrites. *Geochimica et Cosmochimica Acta* 55:67–76.
- Wang, M., & Zhou, L. 2012. Simultaneous oxidation and precipitation of iron using jarosite immobilized *Acidithiobacillus ferrooxidans* and its relevance to acid mine drainage. *Hydrometallurgy*, 125, 152-156.
- Wänke H., Dreibus G., Jagoutz E., 1984. Mantle chemistry and accretion history of the Earth, *Arch. Geochem. Springer-Verlag*, Berlin. 1-24.
- Zolotov, M.Y., 2011. On the chemistry of mantle and magmatic volatiles on Mercury. *Icarus*

212: 24-41.

Tables.

Table 1. Composition of the solution of trace elements added in growth medium (from modified solution of Stergar and Zagorc Koncan, 2002).

Compound	MnCl ₂ ,4 H ₂ O	H ₃ BO ₃	ZnCl ₂	CuCl ₂	Na ₂ MoO ₄ , 2H ₂ O	CoCl ₂ , 6H ₂ O	NiCl ₂ , 6H ₂ O
Mass concentration mg/L	50	5	5	3	1	100	10

Table 2. Initial dissolution rates of troilite, Fe₈₂Si₁₈ alloy, enstatite and synthetic EC during abiotic and biotic experiments with *A. ferrooxidans* (A.F.) and *A. thiooxidans* (A.T.). The temperature was at 20°C under air and atmospheric pressure, the pH was around 2.2 for all experiments except for the enstatite experiments. The initial dissolution rates of enstatite have thus been corrected at pH 2 following Oelkers and Schott (2001). The error due to this correction was around 7%, which was about the same error than the one due to analytical uncertainties.

	Initial dissolution rate (mol/cm ² /s)		
	Abiotic	Biotic with A.F	Biotic with A.T.
Troilite	Fe: 7.8 (±1.6) × 10 ⁻¹¹	Fe: 1.0 (±0.25) × 10 ⁻¹⁰	Fe: 1.2 (±0.3) × 10 ⁻¹⁰
Fe₈₂Si₁₈ alloy	Si: 5.5 (±1.1) × 10 ⁻¹¹	Si: 6.9 (±1.5) × 10 ⁻¹¹	Si: 8.1 (±1.6) × 10 ⁻¹¹
	Fe: 5.9 (±1.2) × 10 ⁻¹⁰	Fe: 5.8 (±1.1) × 10 ⁻¹⁰	Fe: 6.6 (±1.3) × 10 ⁻¹⁰
Enstatite	Si: 1.0 (±0.2) × 10 ⁻¹³	Si: 1.4 (±0.4) × 10 ⁻¹³	Si: 1.3 (±0.3) × 10 ⁻¹³
	Fe: 3.2 (±0.6) × 10 ⁻¹⁴	Fe: 6.0 (±1.3) × 10 ⁻¹⁴	Fe: 6.0 (±1.3) × 10 ⁻¹⁴
	Mg: 1.7 (±0.4) × 10 ⁻¹³	Mg: 2.4 (±0.5) × 10 ⁻¹³	Mg: 2.7 (±0.5) × 10 ⁻¹³
Synthetic EC	Si: 7.8 (±1.7) × 10 ⁻¹¹	Si: 10.0 (±4) × 10 ⁻¹¹	Si: 7.9 (±1.7) × 10 ⁻¹¹
	Fe: 6.2 (±1.3) × 10 ⁻¹⁰	Fe: 9.0 (±1.8) × 10 ⁻¹⁰	Fe: 7.1 (±1.4) × 10 ⁻¹⁰
	Mg: 6.9 (±1.4) × 10 ⁻¹⁰	Mg: 7.0 (±1.5) × 10 ⁻¹⁰	Mg: 4.6 (±1.0) × 10 ⁻¹⁰

Table 3. Pyroxenes dissolution rates at pH 2 found in literature.

Mineral	Compositions	Weathering conditions	Si dissolution rates (mol. cm ⁻² . s ⁻¹)	References
			pH 2	
Diopside	(Ca _{0.8} Mg _{0.8} Fe _{0.2} Al _{0.1}) Si ₂ O ₆	T=25°C	8.8 × 10 ⁻¹⁵	Knauss <i>et al.</i> , 1993
		T=70°C	1.4 × 10 ⁻¹³	Knauss <i>et al.</i> , 1993
		T=25°C	1.3 × 10 ⁻¹⁵	Chen and Brantley, 1998
		T=90°C	9 × 10 ⁻¹⁴	Chen and Brantley, 1998
Anthophyllite	(Mg _{5.7} Fe _{1.0} Al _{0.1}) Si _{7.8} O ₂₂ (OH) ₂	T=25°C	1.3 × 10 ⁻¹⁷	Chen and Brantley, 1998
		T=90°C	9 × 10 ⁻¹⁵	
Wollastonite	CaSiO ₃	T=22.5°C	6 × 10 ⁻¹¹	Rimstidt and Dove, 1986
		T=25°C	6.6 × 10 ⁻¹³	Xie, 1994
Bramble enstatite	(Mg _{1.7} Fe _{0.28} Ca _{0.01})Si ₂ O ₆	T=70°C	3.6 × 10 ⁻¹³	Oelkers and Schott, 2001

Figure captions.

Fig. 1: Sketch of the alteration experiment. Powder (in the case of FeS) was placed in the perforated polypropylene tube whereas bulk samples were at the bottom of the flask. Solids were immersed in 75 mL of aqueous solution.

Fig. 2: Backscattered electron microscope images of synthetic EC meteorite before alteration. All the phases of the sample, are present: enstatite, SiO₂, Fe-Si-rich metallic phase, (Mg, Fe, Ca)S sulfides and troilite.

Fig. 3: Solution concentrations of Mg, Fe and Si (measured by ICP-AES) from synthetic EC as a function of time in abiotic and in biotic experiments. (a) Mg concentration in abiotic (■), biotic with *A. ferrooxidans* (▲), biotic with *A. thiooxidans* (○). (b) Fe. (c) Si. (d) Mg/Si molar ratio plotted as a function of time for the different experiments. (e) Fe/Si molar ratio plotted as a function of time for the different synthetic EC experiments.

Fig. 4: Backscattered and secondary electron scanning microscope images of EC analogue. (a) The EC analogue before and after abiotic alteration. Before alteration, enstatite, metal and (Mg, Fe, Ca)S were present. After alteration (Mg, Fe, Ca)S and metal were replaced by holes (black in the picture) or covered by SiO₂ and sulfates. The surface of enstatite was covered by scarce and tiny crystals of phosphates and sulfates. (b) In a sulfide hole of abiotic alteration, tiny globules of iron oxides/hydroxides and rods of sulfates were observed. (c) In a sulfide hole of biotic alteration with *A. ferrooxidans*, rods of sulfates were observed and show textural differences from the abiotic samples. (d) Before and after biotic alteration with *A. thiooxidans*. Before bioalteration, this part of sample contained enstatite and assemblages of metal, troilite and (Mg,Fe,Ca)S grains. After bioalteration, the surface of enstatite contained sulfates and very rare phosphates. The assemblages of metal-sulfide were totally transformed: there were mainly holes, which contained rods of sulfates, SiO₂ and iron oxides or hydroxides. (e) This photo is a zoom of the right part of (d). In the FeS hole dissolution, there were patches of iron oxides or hydroxides, with tiny globules of elemental sulfur. (f) After biotic alteration with *A. thiooxidans*. In a (Mg,Fe,Ca)S hole, tiny globules of iron oxides or hydroxides and rods of 677 sulfates. (g) Before and after biotic alteration with *A. ferrooxidans*. Before bioalteration, this part of sample contained enstatite and assemblages of metal and troilite. After bioalteration, the surface of enstatite contained few sulfates. The assemblages of metal-troilite were totally transformed: the metal was covered by a SiO₂-layer and the troilite by sulfates and iron oxides or hydroxides. (h) After biotic alteration with *A. ferrooxidans*, the surface of a Fe-Si alloy is totally covered by SiO₂ and small globules of iron oxides 682 or hydroxides. (i) Zoom on the globules of iron oxides or hydroxides of (h). (j) biofilms with a filamentous aspect observed with *A. thiooxidans* on FeS and Fe-Si alloys grains. (k) Three bacterial cells (here with *A. thiooxidans*, in light grey on the photo) observed on the surface of the samples.

Fig. 5: Fe release (measured by ICP-AES) from troilite as a function of time: total Fe concentration: abiotic (■), biotic with *A. ferrooxidans*, (▲) biotic with *A. thiooxidans* (○).

Fig. 6: Backscattered and secondary electron scanning microscope images of troilite after weathering and bioweathering with *A. ferrooxidans* and *A. thiooxidans*. (a) Troilite reacted in abiotic experiment. The surface was completely covered by a thick (~5 μm) secondary phase which was dominated by iron and oxygen. Iron phosphates are also observed. (b) Troilite reacted in biotic experiment with *A. thiooxidans*. The surface was partially covered by a

secondary phase, which formed patches. These patches are composed of iron sulfates. (c) Down in the center of the picture, one bacterial cell (here *A. thiooxidans*) observed on the surface of the “FeS reference experiments”.

Fig. 7: Fe and Si release (measured by ICP-AES) from Fe₈₂Si₁₈ alloy as a function of time. (a) Total Fe concentration in abiotic (■), biotic with *A. ferrooxidans* (▲) and biotic with *A. thiooxidans* (○). (b) Si concentration in abiotic, biotic (with *A. ferrooxidans* and *A. thiooxidans*) experiments. (c) Fe/Si molar ratio in abiotic and biotic experiments.

Fig. 8: Backscattered and secondary electron microscope images of Fe₈₂Si₁₈ alloy after abiotic alteration and bioweathering with *A. ferrooxidans*. (a) Fe₈₂Si₁₈ alloy reacted in abiotic experiment. The half-sphere surface was completely covered by a secondary phase. This secondary phase was a very thick silica layer. Under it, Fe-Si alloy was characterized. (b) Fe₈₂Si₁₈ alloy reacted in biotic experiment with *A. ferrooxidans*. The surface was only partially covered by silica. There were also some thin iron phosphates at the surface of this silica layer, but they were not stable under the SEM beam. Under this layer, Fe-Si alloy and iron oxides and/or hydroxides were observed. (c) Very fine shredded and bent biofilms (light grey) on the surface of the metallic alloy (here with *A. ferrooxidans*).

Fig. 9: pH evolution as a function of time (a) in San Carlos enstatite experiment abiotic (■), biotic with *A. ferrooxidans*, (▲) biotic with *A. thiooxidans* (○). San Carlos enstatite dissolution as a function of time (b) Fe concentration in abiotic and biotic experiments. (c) Mg concentration in abiotic and biotic experiments. (d) Si concentration in abiotic and biotic experiments. (e) Molar Mg/Si ratio as a function of time for the different enstatite experiments (abiotic and biotic). The dissolution of enstatite was not stoichiometric and the Mg/Si (around 2) is very different to the stoichiometric ratio of enstatite (Mg/Si=0.9). (f) Molar Fe/Si ratio as a function of time for the different enstatite experiments (abiotic and biotic).

Fig. 10: Backscattered scanning electron microscope images of San Carlos enstatite millimeter-sized grains after (a) abiotic alteration and (b) bioweathering with *A. ferrooxidans* with numerous etch pits. Etch pits are less numerous and shallower than with *A. thiooxidans* or after abiotic alteration. (c) Several bacterial cells (here *A. ferrooxidans*) observed on the surface of the “Enstatite reference experiments” at the top and bottom of the picture.

Figure 1.

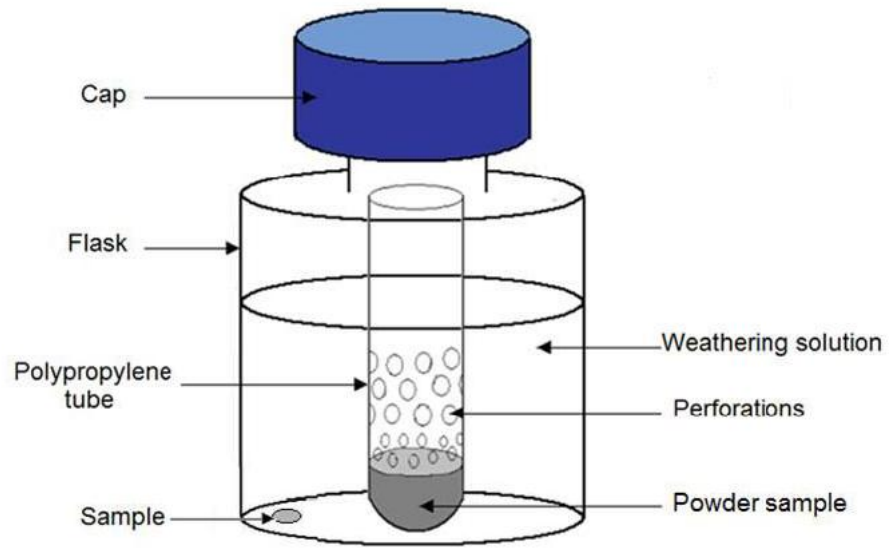


Figure 2

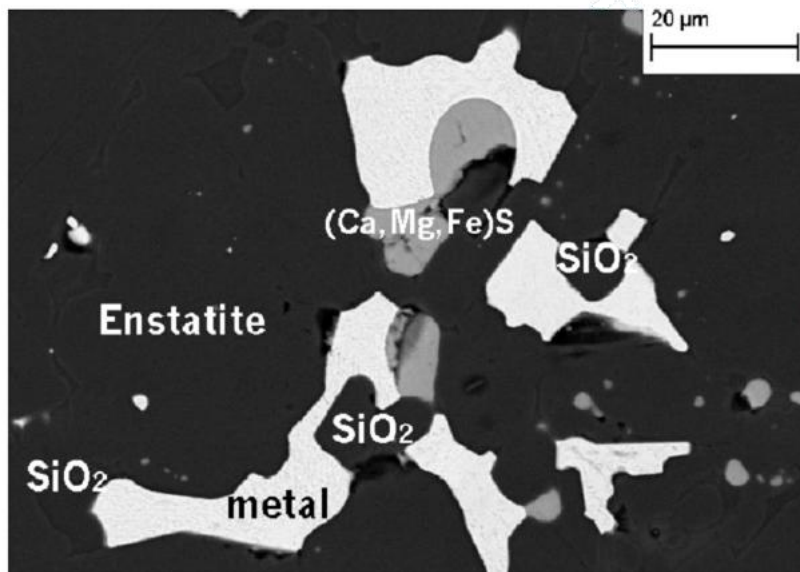
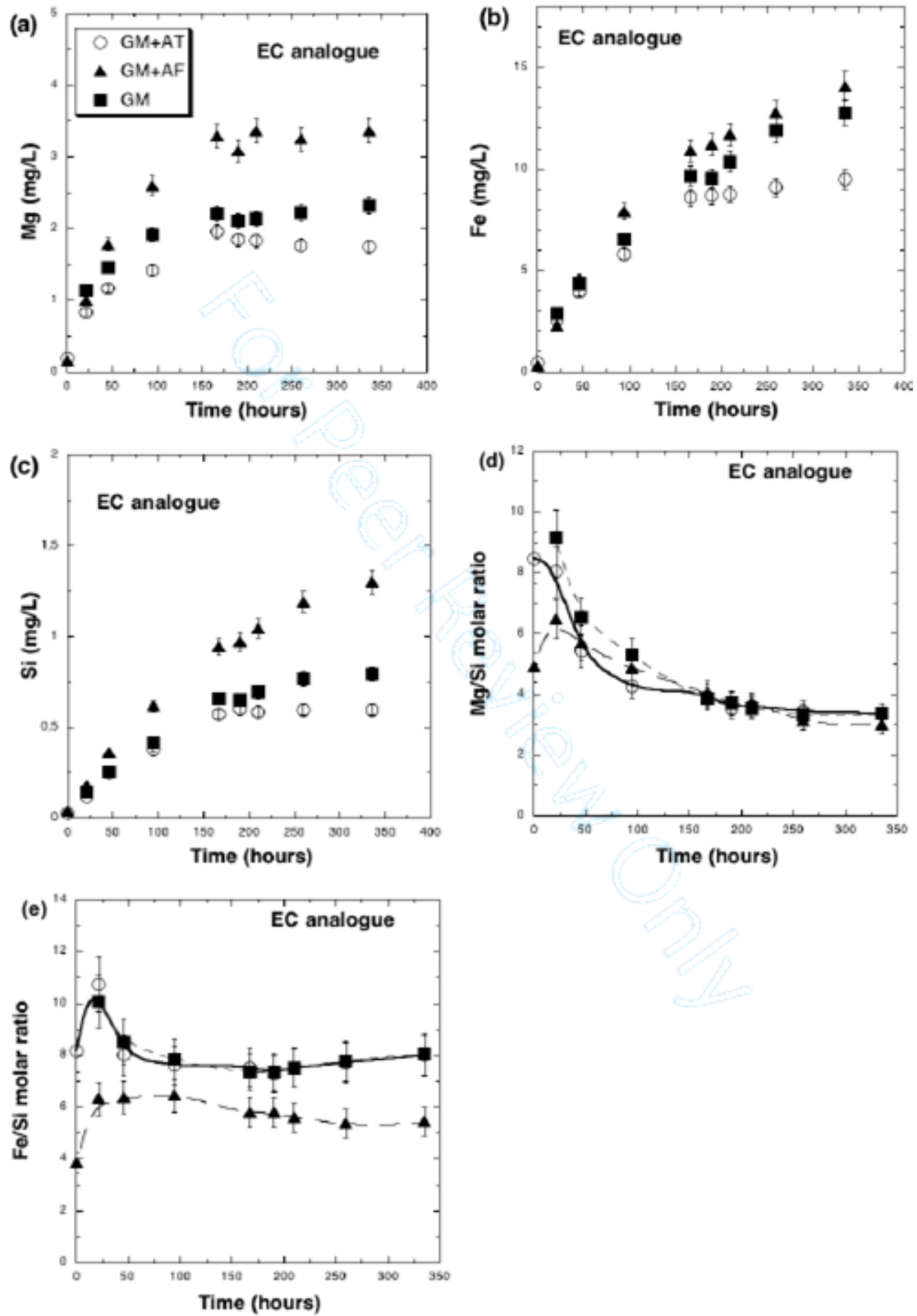
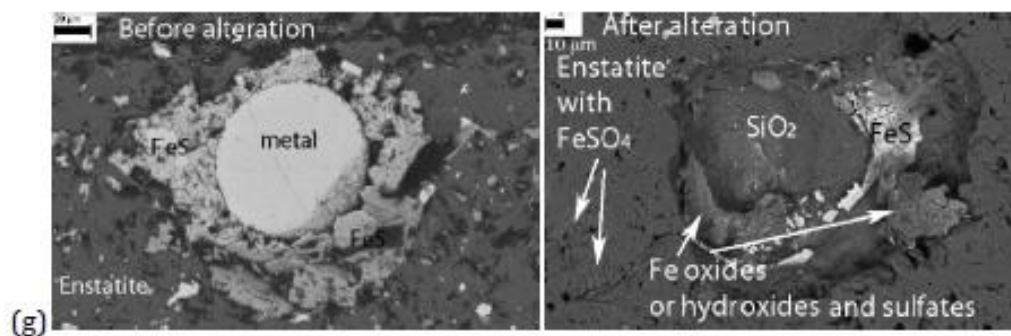
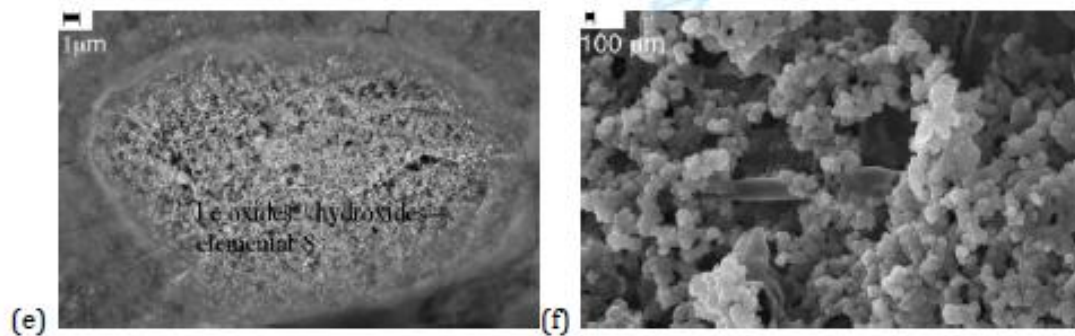
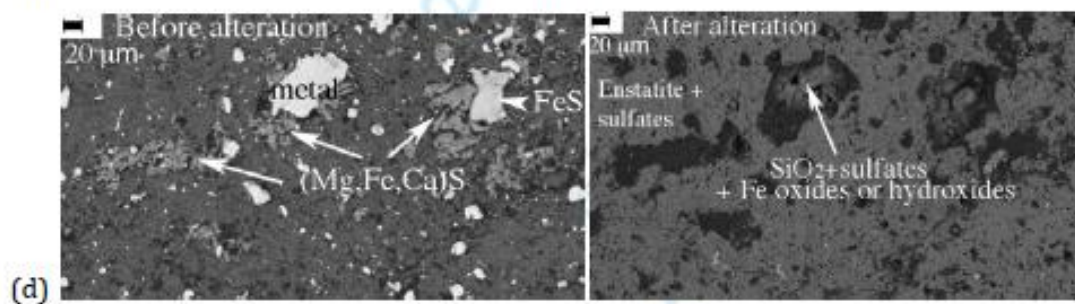
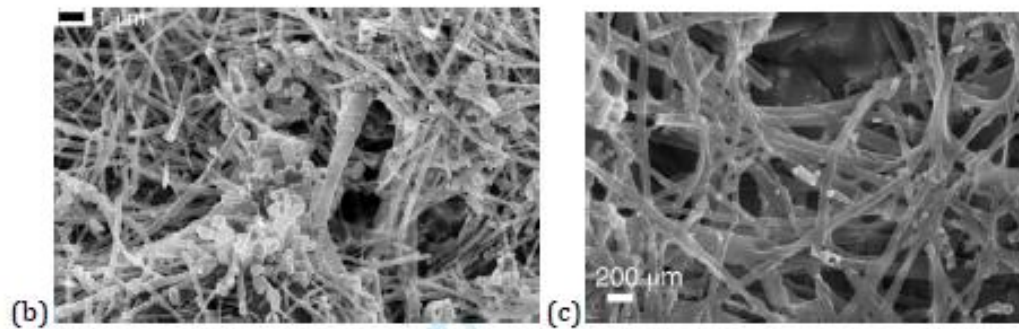
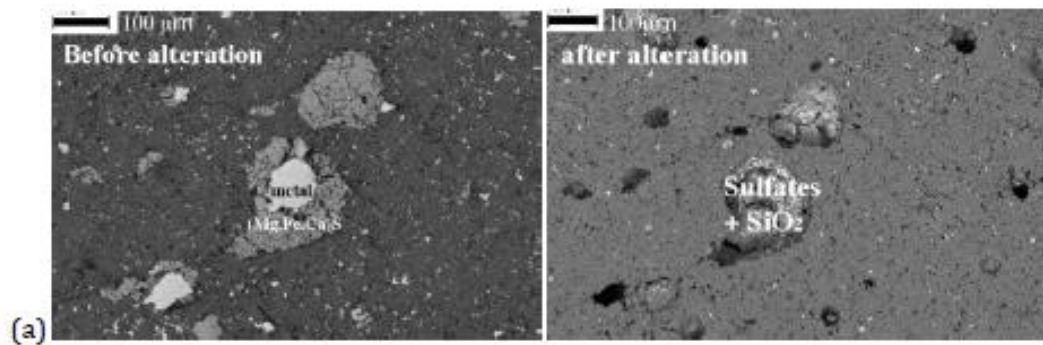


Figure 3.





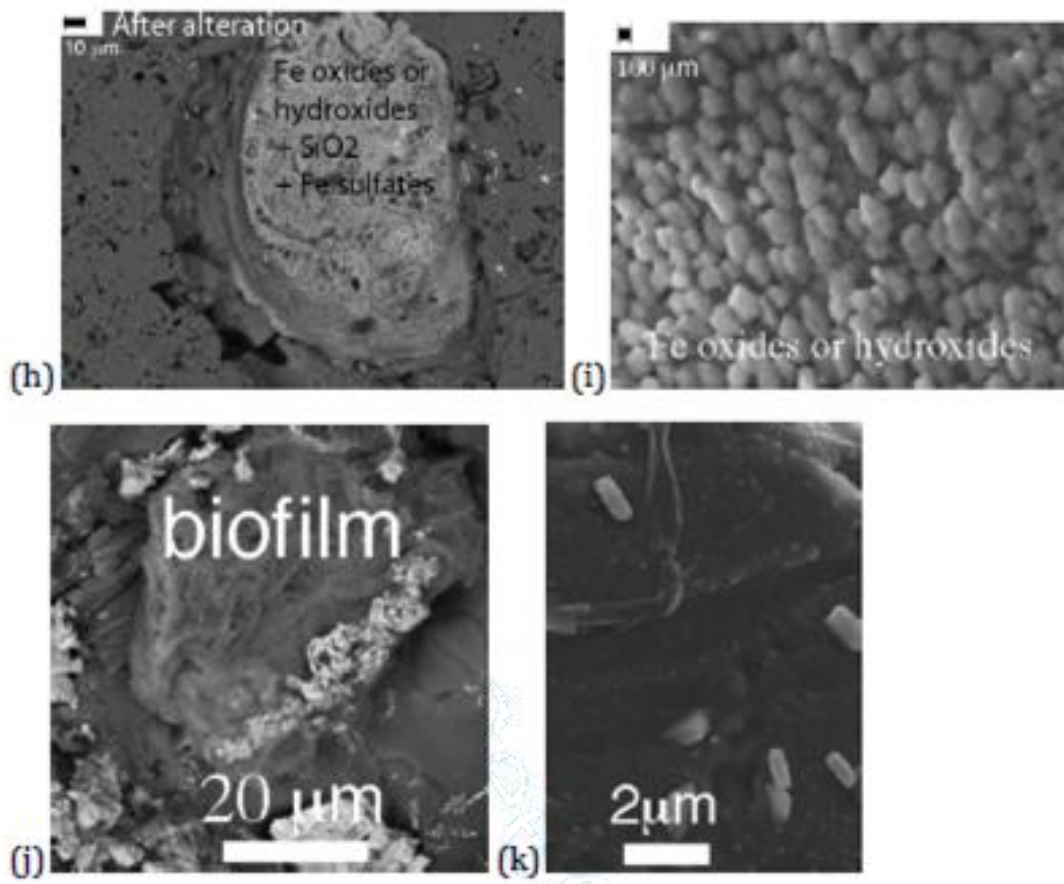


Figure 5

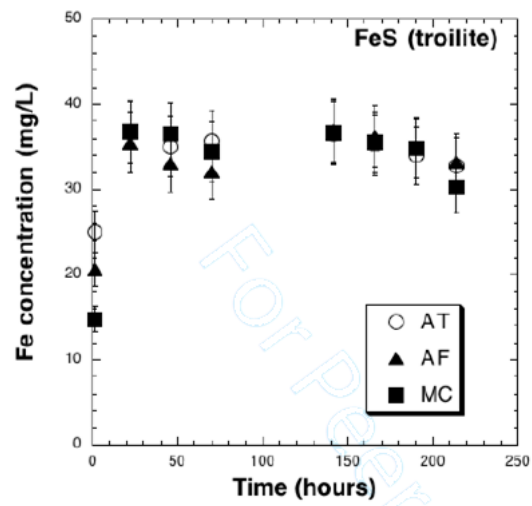


Figure 6

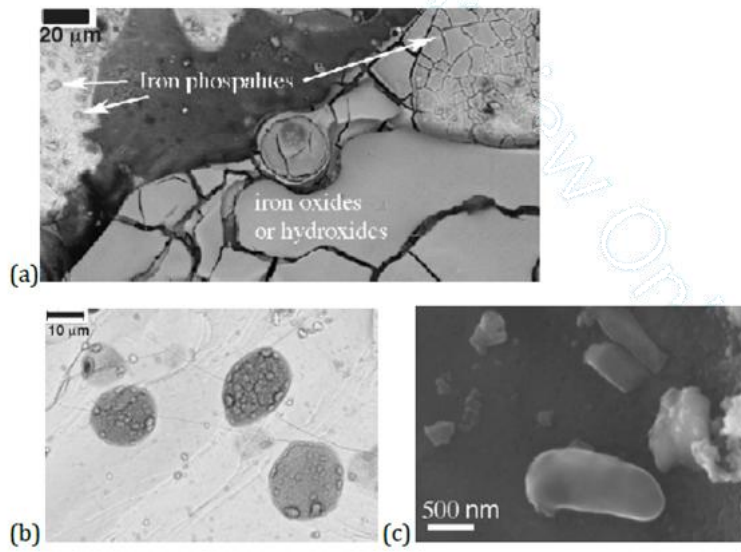


Figure 7

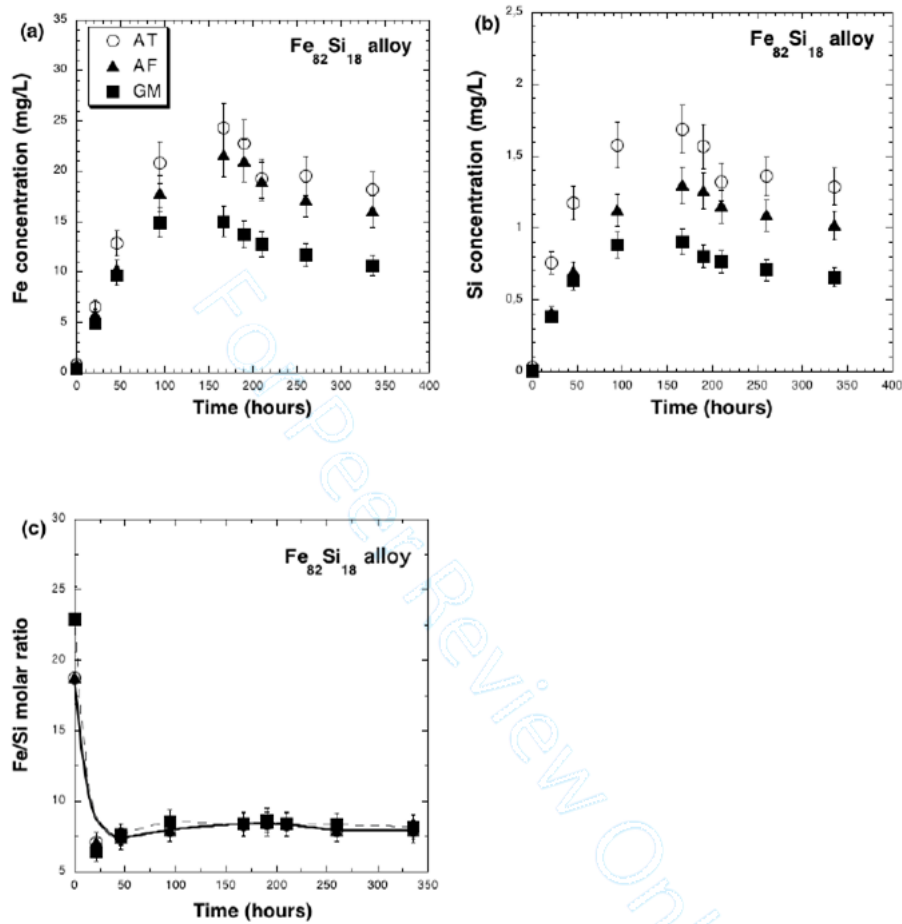


Figure 8.

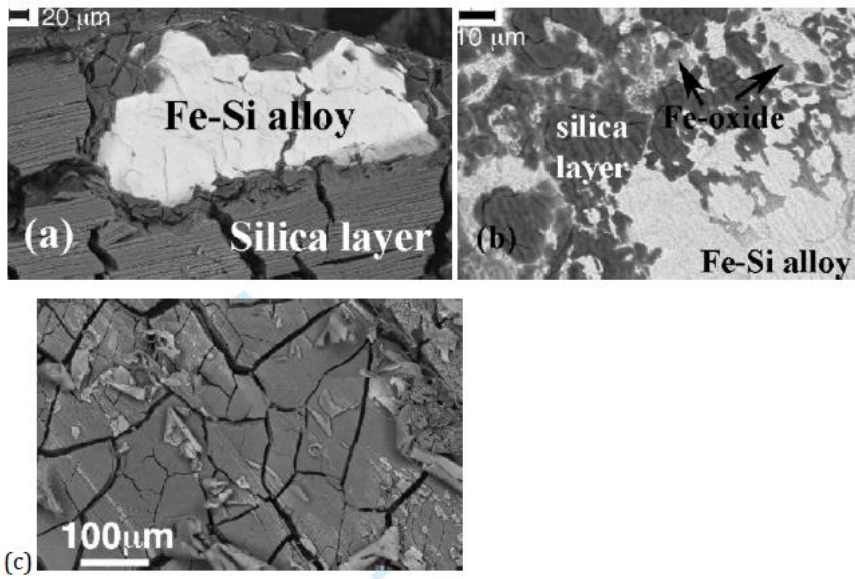


Figure 9

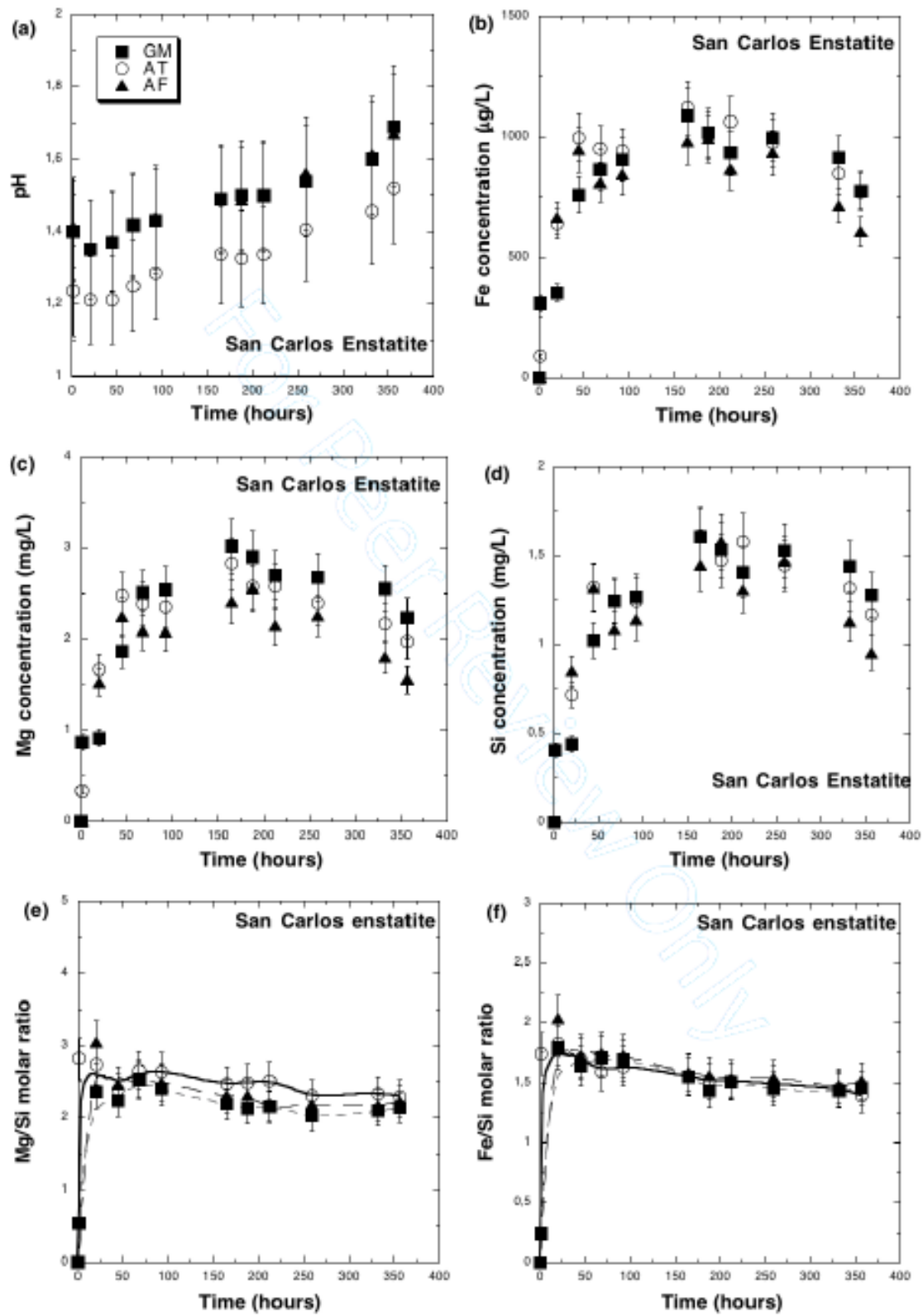


Figure 10

